Shear-Induced Morphologies of Cubic Ordered Block Copolymer Micellar Networks Studied by in Situ Small-Angle Neutron Scattering and Rheology

Kell Mortensen,*,† Elisabeth Theunissen,‡ Ralf Kleppinger,§ Kristoffer Almdal,† and Harry Reynaers‡

Danish Polymer Centre, Risø National Laboratory, Roskilde, Denmark, Laboratory of Macromolecular Structure Chemistry, Katholieke Universiteit Leuven, Leuven, Belgium, and Laboratory of Macromolecular and Organic Chemistry, Eindhoven University of Technology, Eindhoven, The Netherlands

Received December 3, 2001; Revised Manuscript Received June 6, 2002

ABSTRACT: Triblock copolymers in a solvent selective for their middle blocks provide the basis for the formation of novel physical networks in which cross-links are formed by self-assembled domains of the end blocks. Triblock copolymers of poly(styrene)−poly(ethylene butylene)−poly(styrene) (SEBS) dissolved in oil constitute such a network system of thermoplastic elastomer. We present combined mechanical and structural data on such SEBS gels as studied using a Rheometrics RSA-2 instrument modified for in situ measurements of small-angle neutron scattering and rheology. The self-association of the PS blocks not only promotes the formation of highly interconnected end-block domains but, within a given temperature range, constitutes a network with body-centered cubic (bcc) microstructure. The texture of the bcc phase can, within a given temperature window, be controlled in great detail by applying large-amplitude oscillatory shear of specific amplitude and frequency. We map out the shear-induced morphology and show that both {111}/⟨112⟩ and {110}/⟨111⟩ domain texture can be made, where {*hkl*} and ⟨*hkl*⟩ represent the crystal plane and crystal axis parallel to the ($\bar{v}\bar{\nabla}$) shear plane and $\bar{v}$ shear direction, respectively. The thermodynamically stable cubic phase is limited at high-temperature by an order−disorder transition and at low temperature by the glass transition of polystyrene.

I. Introduction

The molecular self-assembly of nanometer-scaled aggregates and ordered mesophases has been studied extensively in recent years.[1,2] Both block copolymer melts and block copolymer molecules suspended in selective solvents provide the basis for such structures because of incompatibility between the various units within the materials. Linear ABA triblock copolymers made up of two A blocks surrounding a B block typically form independent core−corona structured micellar aggregates when mixed with a solvent selective for the A blocks. Micelle formation is caused by a thermodynamically driven reduction in enthalpic energy by the avoidance of direct contact between the B polymer and the solvent.[3,4]

Different characteristics can be expected in systems of triblock copolymers mixed in solvents selective for the middle block. The middle blocks of those copolymers form either loops, starting and ending within the same core, or bridges between different micelles. These bridging chains result in a network of interconnected micellar cores. Examples of such systems are aqueous systems of different poly(oxy alkylene) copolymers, e.g., copolymers of poly(ethylene oxide) and poly(propylene oxide),[5] and organic suspensions of the family of related polymers with poly(styrene) end blocks, and poly(butylene), poly(isoprene), poly(ethylene propylene), or poly(ethylene buthylene) middle blocks.[6−10]

* To whom correspondence should be addressed. E-mail: kell.mortensen@risoe.dk.
† Risø National Laboratory.
‡ Katholieke Universiteit Leuven.
§ Eindhoven University of Technology.

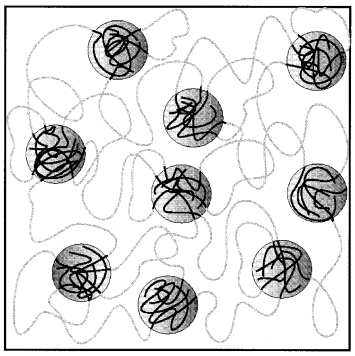

Figure 1. Schematic illustration of the SEBS micellar network structure.

A. SEBS Micellar Networks. The present study concerns the triblock copolymer system of poly(styrene)−poly(ethylene butylene)−poly(styrene), abbreviated SEBS. SEBS constitutes a micellar network system when mixed with organic solvents that are selective for the poly(ethylene butylene) middle block. This has been verified by scattering experiments[7] and successive TEM microscopy studies.[11] The PEB midblock chain is expected to form both loops and bridges between the polystyrene micelles, depending on whether the two PS end blocks are located in the same or in different polystyrene domains. At low temperatures, the polystyrene cores constitute glassy domains. The network structure is therefore permanent, with the micellar cores acting as physical cross-links. Figure 1 shows schematically the micellar network morphology.

Such micellar networks confer attractive material properties on thermoplastic elastomers. At temperatures above the glass transition, they typically have

10.1021/ma0121013 CCC: $22.00 © 2002 American Chemical Society
Published on Web 08/23/2002

relative low viscous mechanical properties that allow easy processing, while at ambient temperature, the materials are solidlike with highly elastic characteristics.

The original scattering studies on SEBS gels showed that the ambient-temperature organization of the spherical micellar PS cores is typically liquidlike.[7,12,13] Extended structural studies performed at temperatures above the glass transition temperature of polystyrene (T_g(PS) $\approx$ 70−80 °C) showed, however, a significant decrease in the structure factor line width. Narrowing of the line width proceeds over 5−10 min of the annealing process, indicating relative slow dynamics in the buildup of some highly correlated micellar organization.[14] Upon successive cooling, the line width does not recover its original breadth but remains narrow. These studies indicate that the structure observed at ambient temperature does not necessarily represent a thermodynamically stable phase, but rather mimics a frozen state with characteristics of the temperature at which it was originally mixed and quenched, whether liquidlike or ordered.

For triblock copolymer concentrations above approximately 10%, additional peaks in the structure factor clearly emerged during the annealing process, indicating true ordering on a bcc lattice.[8,9,14] This ordered bcc morphology undergoes melting at higher temperatures simultaneously with a marked decrease in elastic modulus.[15]

B. Response to Shear. It is well-known that shear can have a dramatic effect on the texture of ordered block copolymer and colloidal systems, including the possibility of forming single-domain crystalline structures.[8,16−22] Some of the first experiments in the field of shear-aligned block copolymer mesophases were actually performed on triblock copolymer systems very close to the one discussed here, but in the bulk.[16,23−26] These early studies concerned mainly the hexagonal rod phase of polystyrene−polybutadiene (PS−PB−PS) and polyisoprene−polybutadiene (PI−PB−PI) block copolymers and focused on the hexagonal packing of cylinder microstructures.

Different shear-induced single-domain oriented morphologies have previously been documented. In lamellar-forming copolymers, three distinct layer alignments have been observed: parallel orientation with the lamellae normal $\bar{n}$ parallel to the shear gradient ($\bar{n} \parallel \bar{\nabla}$), perpendicular orientation with the lamellae normal parallel to the neutral axis ($\bar{n} \parallel \bar{e}$), and transverse orientation with the lamellae normal parallel to the shear flow ($\bar{n} \parallel \bar{v}$).[27−29] We have previously, in collaboration with Bates et al., described the effect of large-amplitude oscillatory shear on the lamellar phase PEP−PEE-PEP triblock copolymer melts[29,30] and shown that coupled shear and temperature can control the lamellar orientation. Extended studies on the lamellar orientations of block copolymer melts have been performed by the groups of Winey,[31,32] Wiesner,[33−35] and Kornfield,[36,37] among others. In the vicinity of the order−disorder transition (ODT) the perpendicular arrangement was shown to be stabilized at high shear rates, whereas at lower shear rates, the parallel alignment was shown to be stable. The cross over from low to high deformation rates was, in analogy with the results of the present study, found to occur near the frequency where G' and G'' become equal. Only well below T_{ODT} was the parallel orientation achieved.

In analogy with the lamellar studies, hexagonal cylinder phases have shown different shear-induced texture, depending on both temperature and strain amplitude.[38,39] Both the {10} orientation of the hexagonal planes and the {11} orientation have, under given circumstances, been observed to align perpendicular to the shear gradient.[3,24,39]

The shear dependence of cubic ordered block copolymer structures has been addressed in a number of studies,[19,38,40−42] but a more general statement on the resulting domain structure is still lacking. In collaboration with Bates et al., we have previously studied the shear response of cubic bcc ordered diblock copolymer melts.[19,38,42] The twinned bcc structure was observed both for shearing directly in the bcc phase and for heating from a shear-oriented hexagonal cylinder phase. With different shear rates, various textures appeared. For sufficiently low shear rates, the bcc domains slip via {110} planes moving along the $\langle \bar{1}11 \rangle$ direction, leaving an almost undisturbed scattering pattern. Shearing at intermediate rates leads to an apparent disordering, as evident from the isotropic Debye−Scherrer scattering. However, after cessation of shear the twinned bcc structure reappears, signifying that, during the application of shear, the {110} planes lose only translational order while maintaining orientational order. Once shearing has ceased, the layers restack, thereby reestablishing crystalline order.[19]

Both cubic ordered micellar and colloidal suspensions have been studied quite extensively in shear fields.[3,20,43−49] Shear-induced morphology changes and lattice deformations have been revealed both in micellar suspensions, as studied by Gast and co-workers,[44] and in charged-stabilized dense colloidal systems, as reported by Ackerson et al.[46,47] Different textures have been reported, including the twin structure often observed in block copolymer melts[41] and single-domain structures.[3] Hamley et al. studied shear dependence rather systematically and found that a shear amplitude of about 100% was needed to change a cubic ordered diblock copolymer gel into macroscopic orientation.[40] They found further that low shear frequencies (ω below 10 rad/s) lead to the predominant alignment of {100} planes with normals parallel to the shear direction, whereas higher shear aligns the $\langle 111 \rangle$ axis parallel to the shear. The latter structure was assumed to be a multigrain structure.

Register and co-workers recently reported rheological and structural data on systems quite similar to those studied by us.[48,49] They found strain- and stress-induced disordering at quite well-defined values. For example, the critical strain for disordering is 0.038 times the shear modulus plateau of the bcc phase. A more detailed comparison to our data is in progress.

The present study reveals details on shear-induced texturing of a micellar triblock copolymer gel, with specific correlation to the rheological characteristics. We have studied a range of SEBS gel systems, including differences in both molecular characteristics (molar mass and PS fraction) and solvents. The systems show qualitatively similar behavior. In the present report, we concentrate on a given SEBS system, Kraton-G1650, and the high-temperature oil Fina A360, as specified below.

II. Experimental Section

The experimental studies concern both structural and mechanical characterizations. A major part of the investiga-

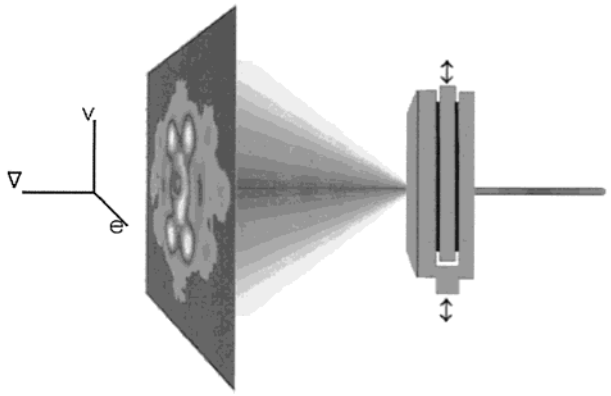

Figure 2. Schematic illustration of the experimental setup, including defenition of principal axes: $\bar{v}$ flow, $\bar{\nabla}$ gradient, and $\bar{e}$ neutral direction.

tions relied on the access to simultaneous structural and mechanical characterization using a rheo−SANS facility.

A. Materials. The triblock copolymer used in the present study is of the SEBS type, that is, poly(styrene)−poly(ethylene butylene)−poly(styrene). The general trends appear to be the same for a variety of SEBS materials, PEB-selective solvents, and SEBS concentrations, but with clear differences in the characteristic transition temperatures.[50] In the present study, we have used the material Kraton G1650 from Kraton Corp./Shell, which has an average molecular mass equal to 100.000 g/mol, a polydispersity index of 1.1,[51] and a polystyrene content of 29%. The solvent selective for the PEB midblock is a high-temperature oil (Fina Vestan A360) based on a mixture of aliphatic and alicyclic compounds with an average molecular mass of around 400 g/mol. The copolymer concentrations were approximately 20%. The SEBS triblock copolymer and the Fina oil were mixed at temperatures well above T_{ODT} (160−180 °C) and stirred until clear solutions were obtained. The suspensions were subsequently quenched to room temperature. This procedure results in transparent, highly elastic materials. The materials were subsequently squeezed between the plates of the shear apparatus at temperatures close to the ODT. Further annealing procedures and temperature stabilization is described in detail below.

B. Rheo−SANS: Rheology and Small-Angle Neutron Scattering. Small-angle scattering experiments were performed at the Risø-SANS facility, using 6-Å neutrons with 9% wavelength resolution. The sample-to-detector distance and the collimation length were both 6 m. The SEBS samples were mounted in a shear sandwich cell in a Rheometrics RSA-2 instrument modified for simultaneous measurements of both dynamic mechanical and structural properties and for studies of structural response to large-amplitude oscillatory shear (LAOS).[45] The elastic and loss moduli (G' and G'', respectively) were obtained with shear amplitude $\gamma = 1\%$ and frequency $\omega = 1$ s^{-1}. Large-amplitude oscillatory shear used for the shear alignment studies were done with shear frequencies in the range $\omega = 0.05-30$ s^{-1} and oscillatory shear amplitudes γ up to 160%. The sample thickness was 0.2 mm. The scattering configuration for the steady shear experiments is outlined in Figure 2. The sandwich was mounted such that the shear velocity direction ($\bar{v}$) was vertical and the shear gradient ($\bar{\nabla}$) horizontal and parallel to the neutron beam. When viewing a two-dimensional diffraction image obtained in this conformation, the shear velocity ($\bar{v}$) is in the vertical direction, and the horizontal direction is parallel to the vorticity vector ($\bar{e}$).

III. Results and Discussion

A. Rheology. At ambient temperature, the SEBS gels constitute a transparent elastic material that typically can be stretched by up to a factor of 10 or more. Figure 3 shows the elastic (G') and loss (G'') moduli of 20 wt % triblock copolymer gel plotted versus temperature. At ambient temperatures, the gels are in a rubberlike

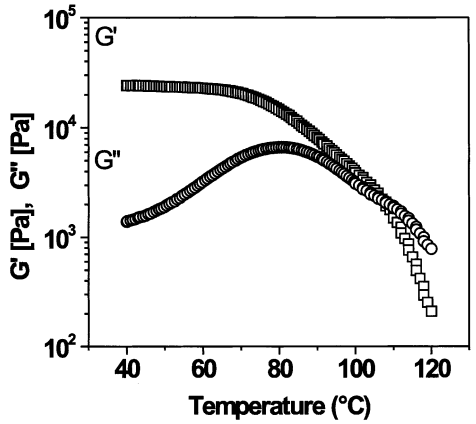

Figure 3. Temperature-dependent shear moduli, G' and G'', of the 20% micellar suspension of SEBS (G1650) in Fina Oil A360. The data were obtained with shear amplitude $\gamma = 1\%$ and frequency $\omega = 1$ Hz.

viscoelastic state in which the polystyrene domains act as permanent physical cross-links.

The mechanical storage modulus (G') is, for the 20% SEBS sample, on the order of 10^4 Pa at ambient temperature. This value remains almost unaffected until the order−disorder temperature of 110−120 °C, although with some decrease near 80 °C. The most significant change observed in the rheological data is the solid-to-liquid type of transition near 110 °C, characterized by significant loss in the elastic modulus and crossing of G' and G''. This transition reflects an order-to-disorder phase transition.[9,15]

In the small-amplitude linear studies, the glass transition is not visible in the elastic properties, but a crossover from a rubbery gel to a plastic fluid is detected close to $T_p \approx 80$ °C. This transition is characterized by a small, but distinct, decrease in G' and a broad maximum in G''. The characteristics are reproducible in temperature also after annealing in the ordered phase. The detailed molecular origin of this 80 °C crossover is still unknown to us. It is quite close to the glass transition temperature of the polystyrene domains, which could lead to speculations on a direct relation to T_g. Other SEBS materials with higher molar masses, however, shows the same characteristics in G' and G'' but at higher temperatures well separated from T_g. More likely, the crossover near $T_p \approx 80$ °C is related to chain dynamics, where the polystyrene blocks start to migrate through thermal motion from one micellar core to another. Such migration is related to both the glass transition temperature and the enthalpic energy of mixing, given by the Flory−Huggins interaction parameter and the molecular size, χN. This explanation is supported by the fact that only above this temperature were we able to detect a gradual formation of well-ordered cubic micellar organization, which, on the other hand, remains when the samples were cooled below both T_p and T_g.[8,9]

The shear frequency and the strain amplitude are factors that play key roles in the formation of single-crystal-type morphologies. Figure 4 shows the elastic characteristics versus frequency in the range 0.05 s^{-1} $< \omega <$ 100 s^{-1} as obtained with 1% shear amplitude in the plastic regime at 90 °C. A characteristic feature is that the storage modulus and the loss modulus are almost equal in the frequency range between 0.9 and 10 s^{-1}. It appears from Figure 11 discussed below that this frequency range is exactly the window where the

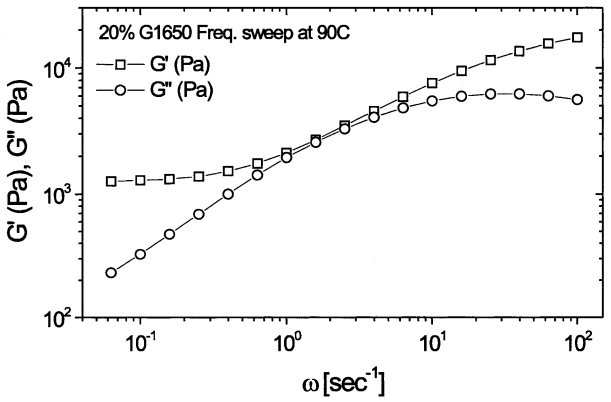

Figure 4. Elastic modulus G' (□) and loss modulus G'' (○) measured versus frequency in a 20% suspension of SEBS G1650 copolymer in Fina A360 oil. The shear amplitude is $\gamma = 1\%$, and the temperature is $T = 90$ °C.

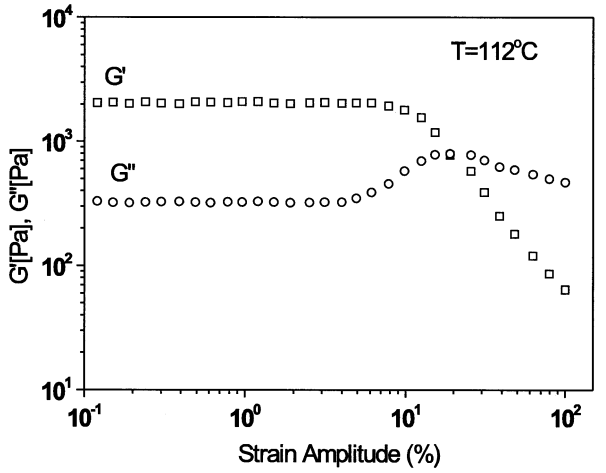

Figure 5. Elastic modulus G' (□) and loss modulus G'' (○) measured versus strain in a 20% suspension in of SEBS G1650 copolymer in Fina A360 oil. The shear frequency is $\omega = 1$ s^{-1}, and the temperature is $T = 112$ °C.

most perfect single- or twin-domain crystal structures can be formed.

Figure 5 shows strain sweep measurements at a temperature of 112 °C. A crossover of G' and G'' can be detected at a strain on the order of 20%. As will be shown below, this is exactly the strain value that is necessary to produce well-defined single-domain texture in the cubic ordered phase.

B. Structural Response to Large-Amplitude Oscillatory Shear. The structural response to large-amplitude oscillatory shear (LAOS) depends critically on the temperature T, shear amplitude γ, and shear frequency ω. Within the window of accessible shear amplitude and frequency, we have not detected any structural changes when shear is applied at temperatures *below* the characteristic crossover temperature T_p giving the change from a rubbery gel to plastic fluid, as discussed above. This is in contrast to results obtained at temperatures above this T_p crossover, where marked texture changes appear within a few cycles of large-amplitude oscillatory shear of a given amplitude and frequency.

An example of the time evolution of the texturing is given in detail in Figure 6, which shows both the evolution of the complex rheological data, G' and G'', and the time-dependent scattering patterns. The data

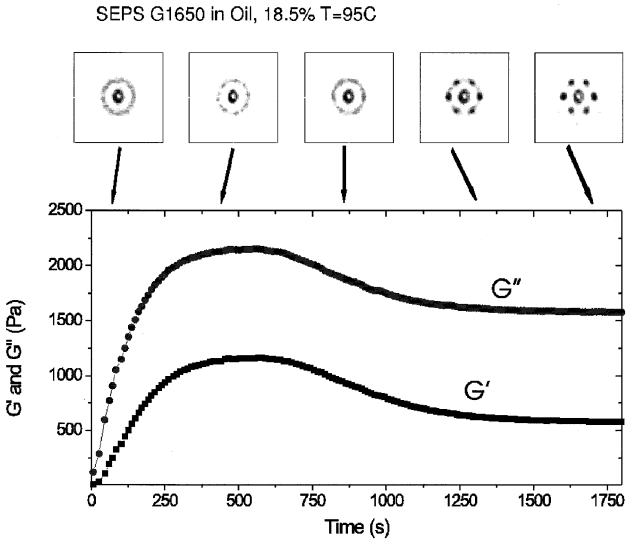

Figure 6. Scattering pattern and shear moduli (G',G'') as obtained simultaneously during large-amplitude oscillatory shear ($\gamma = 40\%$, $\omega = 1$ s^{-1}) at 95 °C. The time = 0 spectrum reflects the structure that is obtained just after quench from the disordered phase at $T \approx 130$ °C.

were obtained during shearing with a strain amplitude of $\gamma = 40\%$ and shear frequency $\omega = 1$ s^{-1}. The sample was quenched from the disordered state just prior to the start of the shear experiment.

Both the storage modulus G' and the loss modulus G'' increase strongly within the first 5 min of the experiment. The scattering patterns within the same time range exhibit minor but distinct changes, expressed in a narrowing of the Debye−Scherrer scattering ring. These changes in both moduli and scattering patterns reflect the slow buildup of an ordered micellar structure. A similar time scale for the kinetics of the ordering process has been suggested in related samples, on the basis of time-resolved X-ray scattering experiments.[14]

During the following 5−10 min, G' and G'' each go through a broad maximum. Simultaneously with the start of the decrease in elastic moduli, texture starts to appear in the scattering patterns, suggesting stress relaxation due to slip along given crystallographic orientations. After about 15 min of shear, a 6-fold symmetric pattern emerges, and the moduli approach a steady-state level. The slip planes of the cubic micellar structure within the given $(\gamma,\omega) = (40\%,1\ \text{s}^{-1})$ experiments are attributed to the crystallographic {111} planes with slip movements along the $\langle 1\bar{1}2 \rangle$ axis.

To map out more detail of the influence of the values of both the oscillatory shear amplitude and the frequency, we present two-dimensional scattering patterns obtained versus γ and ω using different experimental routes.

1. Dependence on Shear Amplitude. Different shear amplitudes were applied on the sample in the plastic fluid regime and the corresponding scattering patterns were obtained and examined. The shear frequency was kept constant at 1 s^{-1}. Data were obtained using two different routes.

One set of data was obtained by applying oscillatory shear without memory effects of earlier applied shear. This was achieved by annealing the sample in the disordered phase at temperatures $T \approx 130$ °C well above T_{ODT}. Afterward, the sample was quenched and stabi-

lized at $T = 95$ °C, and subsequently, the large-amplitude shear was applied to the sample for more than 30 min to secure steady-state conditions (route 1).

A second data set was obtained with large-amplitude oscillatory shear, where the shear amplitude γ was increased stepwise after only 5 min of shear, i.e., without securing either steady-state conditions or disorder between the different γ values (route 2).

Figure 7 shows the scattering patterns obtained in route 1, with shear amplitudes in the range 10−80%. The first column gives the scattering patterns measured during the first 5 min of shear, and the second column gives the patterns obtained during shear after 30 min of shearing. The third column shows the patterns that emerge in the relaxed state after the given oscillatory shear is stopped.

Figure 8 shows the scattering patterns observed as a function of shear amplitude γ ranging from 0 to 160% for the route 2 data set. The first column gives the patterns measured during the 5 min of shear, and the second column gives the patterns that emerge in the relaxed state after the given oscillatory shear is stopped.

It should be emphasized that the data collected during shear in Figures 6−8 represent the integrated patterns as recorded over several shear periodicities.

For experiments that start from disordered micellar configurations (route 1, Figure 7), the scattering patterns obtained within the first minutes of shear all have the same liquidlike profile, namely, an azimuthally isotropic and broad correlation peak centered around $q^* = 0.021$ Å^{-1} (Figure 7). This initially broad ring sharpens within the first 5 min, reflecting the ordering process, and evolves for shear amplitudes $\gamma > 5$−10% into highly anisotropic patterns within a time scale of 15−20 min, as discussed above in relation to Figure 6.

After 30 min of large-amplitude oscillatory shear, a highly ordered texture is formed for most shear amplitudes used. Only the 10% strained sample remains almost isotropic after more than 30 min of shear. With strain amplitudes of more than 10%, on the other hand, marked textures appear related to more or less perfect alignment of the bcc-ordered grains.

The scattering patterns obtained with low strain amplitude (γ in the range 20−30%) are characterized by two strong equatorial peaks (along the $\bar{e}$ direction) and four weaker peaks that grow during the shearing. The two sets of weak peaks merge during relaxation after cessation of shear into two azimuthally broad peaks, centered around the vertical flow axis. This results in a characteristic pattern of four peaks, two strong and azimuthally narrow horizontal peaks and two azimuthally broad vertical peaks. This is in contrast to the cases with larger γ values where the scattering patterns are characterized by spatially highly resolved Bragg peaks.

The nearly 4-fold pattern is in agreement with a texture of the bcc crystals dominated by a crystal orientation with the {001} planes perpendicular to the shear gradient and the ⟨110⟩ axis parallel to the flow $\bar{v}$, i.e., the {001}/⟨110⟩ alignment, see Figure 9. Only the crystallographic ⟨110⟩ axis parallel to the neutral $\bar{e}$ axis is well-defined, however. The azimuthal distribution near the vertical axis suggests that scattering from {111}/⟨$\bar{1}\bar{1}$2⟩ planes is also present, indicating some degree of two-dimensional powder averaging with only the horizontal ⟨1$\bar{1}$0⟩ axis well-defined. During shearing, the {111}/⟨$\bar{1}\bar{1}$2⟩ slip system is apparently the dominant

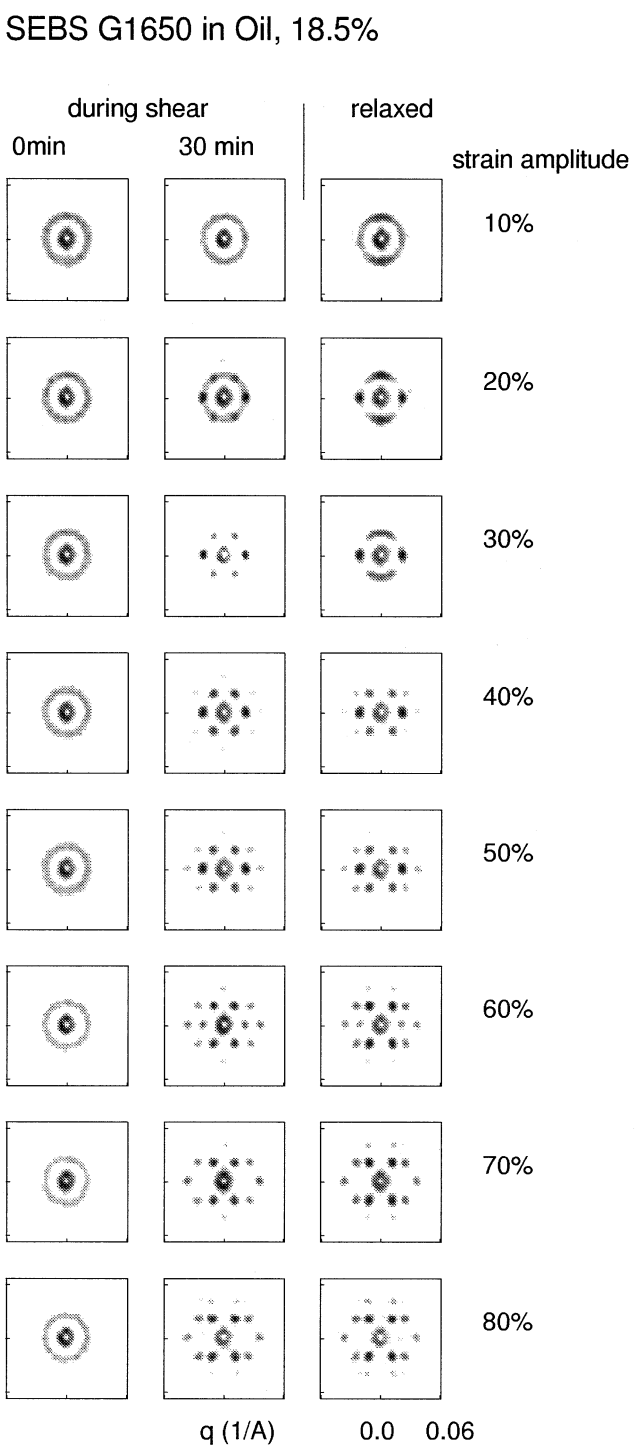

Figure 7. Scattering patterns of 18.5% SEBS G1650 in Fina oil obtained during shear and after relaxation for shear amplitudes in the range $\gamma = 10$−80%, measured with fixed shear frequency $\omega = 1$ s^{-1} and temperature $T = 95$ °C. The first row gives patterns of integrated intensity obtained within the first 5 min of shear, the second row presents the corresponding data obtained after 30 min of shear, and the third column represents the scattering patterns of relaxed sample after shear has been stopped. The sample was annealed ($T > T_{ODT}$) between the experiments of a given shear amplitude to make it isotropic without memory effects.

one. (A more elaborate discussion of the {111}/⟨$\bar{1}\bar{1}$2⟩ orientation is given below.) The mechanism of relaxation from dominating {111}/⟨1$\bar{1}$2⟩ slip system during shear to dominating {001}/⟨110⟩ in the relaxed state is not clear, but it should be emphasized that the {111}/⟨$\bar{1}\bar{1}$2⟩

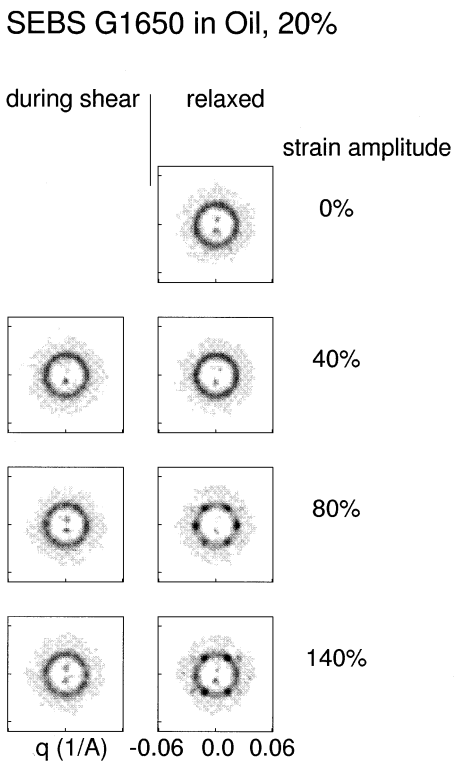

Figure 8. Scattering pattern of 20% SEB -G1650 in Fina oil obtained during shear and after relaxation for shear amplitudes in the range $\gamma = 0-160\%$ for shear frequency $\omega = 1\ s^{-1}$ and temperature $T = 95$ °C. The measurements were done sequentially by increasing the shear amplitude without making the sample isotropic in between (route 2, as described in the text).

type of scattering is obtained during oscillatory shear and might be affected by stretched configurations.

The scattering patterns obtained with intermediate strain amplitude, γ in the range of 40−60%, resemble the low-strain-amplitude patterns discussed above but continue to exist also after relaxation. The pattern can be associated with a bcc structure with {111} sliding planes and the shear velocity ($\bar{v}$) coinciding with the $\langle 1\bar{1}\bar{2}\rangle$ direction, as shown in Figure 9b. This gives the vorticity vector ($\bar{e}$) parallel to the $\langle 1\bar{1}0\rangle$ direction of the bcc domain and the shear gradient ($\bar{\nabla}$) parallel to the $\langle 111\rangle$ direction. The pattern is characterized by 60° opening angles between the six Bragg peaks. It is not possible from the characteristic 6-fold symmetric scattering pattern to judge whether the sample is a true single-domain oriented $\{111\}/\langle 1\bar{1}2\rangle$ crystal or possibly a twin structure. In analogous suspensions of unconnected di- and triblock copolymer micelles, single-domain structures have been suggested from three-dimensional crystallography,[3] and it is likely that the SEBS system has similar single-domain properties. Preliminary studies indicate a $\{111\}/\langle 1\bar{1}2\rangle$ oriented twin structure, with common $\{11\bar{2}\}$ planes parallel to the $\{\bar{v}\bar{\nabla}\}$ plane. This twin structure is similar to that obtained at high strain amplitude, discussed below, but rotated 90° around the $\langle 112\rangle$ axis.

The 6-fold scattering pattern can, of course, also emerge from more complex mixtures of different shear directions. Koppi et al.[19] and Hamley et al.[40] suggested that equivalent scattering pattern observed in block copolymer micellar melts and solutions, respectively, were the results of three principal slip systems: $\{110\}/\langle\bar{1}11\rangle$, $\{211\}/\langle\bar{1}11\rangle$, and $\{321\}/\langle\bar{1}11\rangle$. The same principal slip systems are seen in bcc metals.

Gast and co-workers have studied polystyrene-polyisoprene diblock copolymer micellar suspension, and found scattering patterns that are somewhat alike those presented here.[44] Both low and intermediate shear rates showed six-spot scattering patterns. These patterns were, however, interpreted in terms of a hexagonal close-packed (hcp) phase with strongly distorted {110} planes, resembling a two-dimensional morphology. Ackerson et al. showed that a charged-stabilized dense colloidal suspension can also order on a corresponding twinned fcc lattice when a small shear amplitude is applied, whereas large shear amplitudes cause the formation of close-packed zigzag structure with closest packing along the ($\bar{v}$) velocity axis.[46] An explanation such as that proposed by Ackerson, implying deformed nonequilibrium close-packed structures, is believed not to be valid for the SEBS gels presented here. The bcc phase is stable without shear, so a possible close-packed shear-induced morphology should relax to the bcc structure at rest. The 6-fold symmetric pattern that remains after shear cessation is therefore more likely to represent a true bcc morphology, namely, that with crystal orientation $\{111\}/\langle 1\bar{1}2\rangle$ as discussed above. Shear-induced structural changes somewhat analogous to those proposed by Ackerson and Gast have actually been observed in SEBS micellar gels. In the G1650 material, such a shear-induced bcc-to-hcp (or -fcc) transformation is observed at higher copolymer concentrations, as will be presented elsewhere.[52]

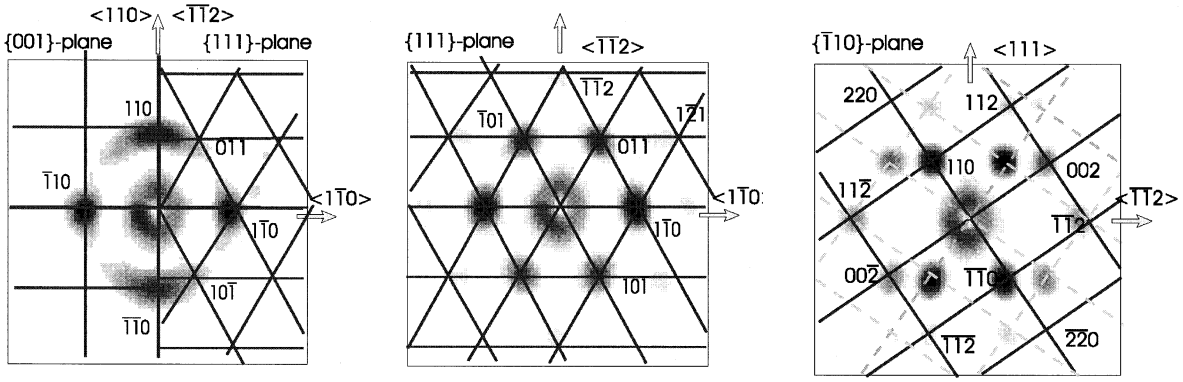

Figure 9. Different scattering patterns observed in the $\bar{v}-\bar{e}$ scattering plane, where the velocity direction $\bar{v}$ is vertical and $\bar{e}$ is horizontal. Pattern a resembles a two-dimensional powder with both $\{001\}/\langle 110\rangle$ (indexed at left) and $\{111\}/\langle 1\bar{1}2\rangle$ ordered (indexed at right) morphologies. The latter is shown in its pure form in pattern b. Pattern c is the bcc twin morphology $\{110\}/\langle 111\rangle$, as illustrated by indexing selected Bragg reflections.

The scattering patterns obtained with high strain amplitude, $\gamma > 70\%$, result in a very well-resolved twinned bcc morphology. This is perhaps the most well-established shear-induced texture of bcc crystals, including both atomic and molecular crystals. In the twin structure, the $\{\bar{1}10\}$ planes are forced to stack normal to the shear gradient and slide relative to each other with a common $\langle 111\rangle$ direction parallel to the shear flow $\bar{v}$ (Figure 9). The boundary between the twins is a common $(\bar{1}\bar{1}2)$ plane normal to the neutral direction of shear, $\bar{e}$.

The structural data for the sample obtained with sequentially increased oscillatory shear (route 2, Figure 8) show essentially the same features, although with a slight difference in the characteristic values of the shear amplitude γ versus scattering pattern. The different orientations of the bcc crystal start to build up at somewhat larger shear amplitudes compared to those of route 1. For example, 60% strain has to be applied in route 1 to create the bcc twin and 140% strain in route 2. This difference is most probably related to the difference in duration of the applied stress: in route 1, the oscillatory shear is applied for more than 30 min and represents a steady-state situation under shear. In route 2, the sample endures only 5 min of large-amplitude oscillatory shear and is still in the transient state of shear alignment. From Figures 6 and 7, it is clear that the single- or twin-domain pattern evolve only after more than 10 min of shear. Moreover, from Figure 7, it appears that the memory of a previous shear amplitude has only a minor influence on the final texture, at least as long as the new shear has an amplitude γ larger than the preceding shear.

Another remarkable observation is that, during the first minutes of shear after a preceding relaxation, an apparent homogeneous Debye−Scherrer ring reappear. This signifies that the first response to shear involves basically all planes parallel to the sliding plane taking part in the sliding mechanism. This causes loss of the translational order but maintenance of the orientational order, as schematically shown in Figure 10. Once shearing has ceased, the layers easily restack, thereby reestablishing three-dimensional crystalline order. From the results of Figure 7, however, we know that, after long-time shear, a state with well-resolved texture is also formed. The sliding mechanism thus changes from all layers taking part at early times to a steady-state situation in which large domains slide relative to each other with only a few sliding dislocations, as sketched in Figure 10. In addition to these mechanisms, there might be some lattice deformation taking place as a response to the macroscopic strain. Such strain-induced oscillatory deformations have been observed in phase-resolved X-ray experiments by Hashimoto et al.[53] With our present instrumentation, we have not been able to resolve similar time-dependent deformations in the SEBS gels.

In works with Bates et al., we found somewhat related shear responses in cubic bcc-ordered diblock copolymer melts.[19] The twinned bcc structure was observed both when shearing directly in the bcc phase, and when heating from a shear oriented hexagonal cylinder phase. Shearing at intermediate rates caused, in analogy with the short-time exposure presented here, an apparent disordering, as is evident from the isotropic Debye−Scherrer scattering. After the shear is stopped, the twinned bcc structure reappears, signifying that, during shear, the {110} sliding planes have lost translational order while maintaining orientational order.

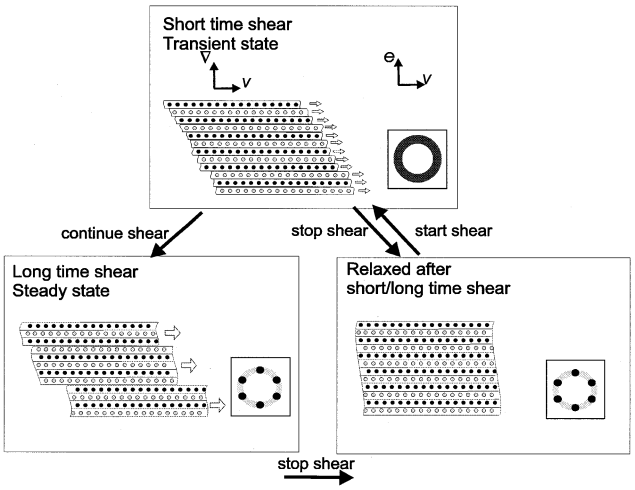

Figure 10. Schematic description of sliding mechanism aftershort-time and long-time exposures to shear. After short-time shearing, all planes take part in the sliding mechanism, leading to loss of translational order but preservation of orientational order of the sliding planes. After long-time exposure, a few dislocation planes emerge, leaving large domains to slide and thus also preserve a high degree of translational order. After cessation of shear, the sliding planes relax in the preferred position giving true three-dimensional crystals that are, to first approximation, independent of the preceding time of shear.

Ackerson et al. also found somewhat related features in a charged colloidal system.[54] For very small shear rates, it was shown that the lattice evolved from a crystalline state in equilibrium to a polycrystalline state, whereas at high shear rates, partial close-packed order was reestablished with the apparent appearance of sliding layer flow.

2. Structural Response to Shear Frequency. Up to now, the large-amplitude oscillatory shear experiments in which single- or twin-domain bcc morphologies were formed were recorded with shear frequency $\omega = 1\ s^{-1}$. To map out the effect that the frequency ω has on the resulting texture, we applied large-amplitude oscillatory shear with ω values in the range of $0.05-30\ s^{-1}$. Figure 11 shows the scattering patterns obtained with a strain amplitude of 80% and at a temperature of 95 °C. The sample was first heated to the disordered phase above T_{ODT}, annealed for about 5 min, and subsequently quenched to 95 °C. Figure 11 shows the scattering patterns obtained during the first 5 min of shear, after 30 min of shear, and after relaxation for the different shear frequencies. A homogeneous Debye−Scherrer pattern is observed both during shear and after relaxation for shear frequencies up to $0.5\ s^{-1}$. Applying a frequency of $\omega = 1\ s^{-1}$ and a strain amplitude of 80% results, as already discussed above, in the formation of the twinned $\{110\}/\langle\bar{1}11\rangle$ morphology. For higher frequencies ($\omega = 5-30\ s^{-1}$), the domain morphology associated with the bcc $\langle 1\bar{1}1\rangle$ axis aligned parallel to the shear gradient and the $\langle\bar{1}\bar{1}2\rangle$ axis parallel to the shear velocity is formed. This is the same texture as was formed with shear frequency of $\omega = 1\ s^{-1}$ and lower strain amplitude strains, as discussed above and shown in Figure 9.

At the highest oscillation rates, $\omega = 30\ s^{-1}$, only the two (110) peaks in the vorticity direction remain strong after relaxation. This signifies the presence of significant

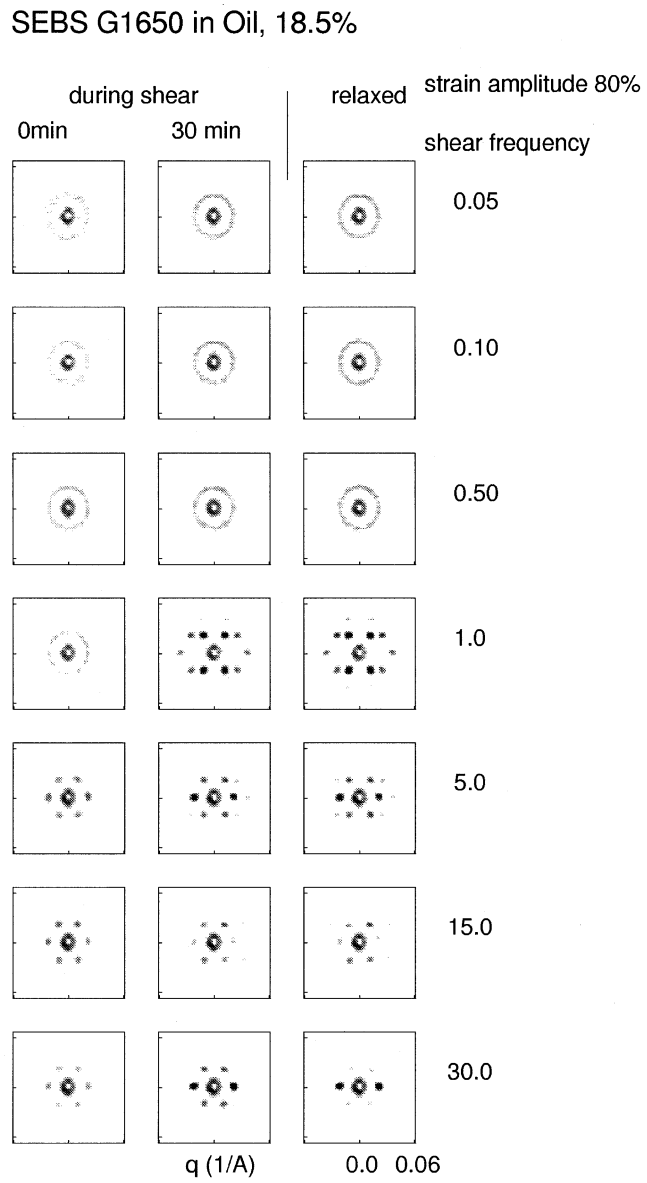

Figure 11. Scattering patterns during shear and after relaxation for different shear frequencies in the range 0.05−30 s^{-1} with a shear amplitude of 80%. The measurements were done sequentially by increasing the shear amplitude without making the sample isotropic in between.

amounts of dislocations in the form of lost translational order between planes perpendicular to the $\bar{e}$ axis.

IV. Conclusions

In summary, we have demonstrated that the use of rheological instruments in situ with SANS facilities provides the basis for detailed insight into the dynamics of texture formation in complex thermoplastic block copolymer systems. it has been shown that shear deformation of triblock copolymer micellar networks promotes the formation of highly ordered morphologies. The rearrangement takes place despite the restrictions that interdomain bridging impose on the mobility of individual micelles.

The shear-induced bcc texture can be summarized in a (γ,ω) diagram (Figure 12), showing the morphologies that emerges after cessation of shear with the given (γ,ω) values. (The same diagram actually also holds for the steady-state shear condition.) At low γ and/or ω

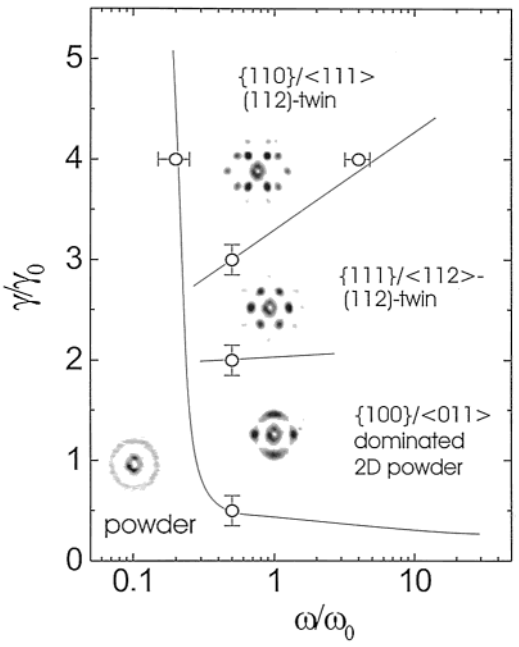

Figure 12. $\gamma-\omega$ phase diagram, showing the development of texture for normalized shear amplitude and shear frequency, where the normalization values $\omega_o = 2\ s^{-1}$ and $\gamma_o = 20\%$ are the values at which the loss modulus G'' crosses or approaches the elastic modulus G' (see Figures 4 and 5).

values, no shear alignment takes place. For small strain amplitudes, γ in the range between approximately 10 and 40% and frequency in the range $1 < \omega < 10\ s^{-1}$, a 2d powder emerges, dominated by the {100}/⟨011⟩ sliding plane configuration. For intermediate strain amplitudes, a {111}/⟨$\bar{1}\bar{1}$2⟩-oriented twin-domain morphology is observed. The largest strain experiments result in the {110}/⟨$\bar{1}$11⟩ twin bcc texture.

The obtained results show that the formation of the bcc single and twin morphologies is constrained to a relative small (γ,ω) window. The measurements demonstrate that the creation of a single or twin morphology is restricted to the frequency range for which the loss modulus G'' approaches the storage modulus G'. This coincidence of a high degree of orientational order and a high loss modulus is really not a surprising result. Both phenomena reflect major slippage along well-defined crystallographic orientations. Analogous results have been described for lamellar systems, where the crossover from low to high deformation rates occur near the frequency where G' and G'' become equal.[27,29]

Acknowledgment. This research program was financially supported by the EU-TMR program for large facilities. E.T. acknowledges FWO-Vlaanderen for a research position.

References and Notes

(1) Hamley, I. W. *The Physics of Block Copolymers*; Oxford University Press: Oxford, U.K., 1988.
(2) Mortensen, K. Structural studies of polymer systems using small-angle neutron scattering. In *Advanced Functional Molecules and Polymers*; Nalwa, H. S., Ed.; Gordon & Breach Science Publishers: New York, 2001; Vol. 2, Chapter 8, pp 223−269.
(3) Mortensen, K. *J. Phys. Cond. Matter* **1996**, *8*, A103−124.
(4) Mortensen, K. *Colloids Surf. A: Physicochem. Eng. Aspects* **2001**, *183−185*, 277−292.
(5) Mortensen, K. *Macromolecules* **1997**, *30*, 503−507.
(6) Raspaud, E.; Lairez, D.; Adam, M.; Carton, J. P. *Macromolecules* **1996**, *29*, 1269−1277.

(7) Mischenko, N.; Reynders, K.; Mortensen, K.; Scherrenberg, R.; Fontaine, F.; Graulus, R.; Reynaers, H. *Macromolecules* **1994**, *27*, 2345−2347.
(8) Kleppinger, R.; Reynaers, H.; Mischenko, N.; Overbergh, N.; Koch, M. H. J.; Mortensen, K.; Reynears, H. *Macromolecules* **1997**, *30*, 7008−7011.
(9) Kleppinger, R.; Mischenko, N.; Theunisssen, E.; Reynaers, H.; Koch, M. H. J.; Almdal, K.; Mortensen, K. *Macromolecules* **1997**, *30*, 7012−7014.
(10) Mortensen, K.; Almdal, K.; Theunissen, E.; Reynaers, H.; Kleppinger, R. *Polym. Mater. Sci. Eng.* **2001**, *85*, 117−118.
(11) Laurer, J. H.; Bukovnik, R.; Spontak, R. J. *Macromolecules* **1996**, *29*, 5760−5762.
(12) Reynders, K.; Mischenko, N.; Mortensen, K.; Overbergh, N.; Reynaers, H. *Macromolecules* **1995**, *28*, 8699−8701.
(13) Mischenko, N.; Reynders, K.; Koch, M. H. J.; Mortensen, K.; Pedersen, J. S.; Fontaine, F.; Graulus, R.; Reynaers, H. *Macromolecules* **1995**, *28*, 2054−2062.
(14) Kleppinger, R.; Mischenko, N.; Reynaers, H.; Koch, M. H. J. *J. Polym. Sci. B: Polym. Phys.* **1999**, *37*, 1833−1840.
(15) Mortensen, K.; Almdal, K.; Kleppinger, R.; Mischenko, N.; Reynaers, H. *Physica B: Condens. Matter* **1998**, *241*−*243*, 1025−1028.
(16) Keller, A.; Pedemonte, E.; Willmounth, F. M. *Nature* **1970**, *225*, 538−540.
(17) Watenabe, H.; Kotaka, T.; Hashimoto, T.; Shibayama, M.; Kawai, H. *J. Rheol.* **1982**, *26*, 153−179.
(18) Ackerson, B. J.; Clark, N. A. *Phys. Rev. A* **1984**, *30*, 906−918.
(19) Koppi, K. A.; Tirrell, M.; Bates, F. S.; Almdal, K.; Mortensen, K. *J. Rheol.* **1994**, *38*, 999−1027.
(20) Mortensen, K.; Brown, W.; Nordén, B. *Phys. Rev. Lett.* **1992**, *68*, 2340−2343.
(21) Eiser, E.; Molino, F.; Porte, G.; Diat, O. *Phys. Rev. E* **2000**, *61*, 6759−6764.
(22) Hamley, I. *Philos. Trans. R. Soc. A: Math. Phys. Eng. Sci.* **2001**, *359*, 1017−1044.
(23) Albalak, R. J.; Thomas, E. L. *J. Polym. Sci. B: Polym. Phys.* **1993**, *31*, 37−46.
(24) Hadziioannou, G.; Mathis, A.; Scoulios, A. *Colloid Polym. Sci.* **1979**, *257*, 136−139.
(25) Morrison, F. A.; Winter, H. H.; Gronski, W.; Barnes, O. D. *Macromolecules* **1990**, *23*, 4200−4205.
(26) Winter, H. H.; Scott, D. B.; Gronski, W.; Okamoto, S.; Hashimoto, T. *Macromolecules* **1993**, *26*, 7236−7244.
(27) Koppi, K. A.; Tirrell, M.; F. S: Bates, Almdal, K.; Colby, R. H. *J. Phys. II (France)* **1992**, *2*, 1941−1959.
(28) Okamoto, S.; Saijo, K.; Hashimoto, T. *Macromolecules* **1994**, *27*, 5547−5555.
(29) Tepe, T.; Hajduk, D. A.; Hillmyer, M. A.; Weimann, P. A.; Tirrell, M.; Bates, F. S.; Almdal, K.; Mortensen, K. *J. Rheol.* **1997**, *41*, 1147−1171.
(30) Hajduk, D. A.; Tepe, T.; Takenouchi, H.; Tirrell, M.; Bates, F. S.; Almdal, K.; Mortensen, K. *J. Chem. Phys.* **1998**, *108*, 326−333.
(31) Winey, K.; Patel, S. S.; Larson, R. G.; Watenabe, H. *Macromolecules* **1993**, *26*, 4373−4375.
(32) Patel, S. S.; Larson, R. G.; Winey, K. I.; Watenabe, H. *Macromolecules* **1995**, *28*, 4313−4318.
(33) Zhang, Y.; Wiesner, U.; Spiess, H. W. *Macromolecules* **1995**, *28*, 778−781.
(34) Zhang, Y.; Wiesner, U.; Spiess, H. W. *J. Chem. Phys.* **1995**, *103*, 4784−4793.
(35) Zhang, Y.; Wiesner, U.; Yang, Y.; Pakula, T.; Spiess, H. W. *Macromolecules* **1996**, *29*, 5427−5431.
(36) Gupta, V. K.; Krishnamoorti, R.; Kornfield, J. A. *Macromolecules* **1995**, *29*, 4464−4474.
(37) Gupta, V. K.; Krishnamoorti, R.; Chen, Z. R.; Kornfield, J. A.; Smith, S. D.; Satkowski, M. M.; Grothaus, J. T. *Macromolecules* **1996**, *29*, 875−884.
(38) Bates, F. S.; Koppi, K. A.; Tirrell, M.; Almdal, K.; Mortensen, K. *Macromolecules* **1994**, *27*, 5934−5936.
(39) Tepe, T.; Schultz, M. F.; Zhao, J.; Tirrell, M.; Bates, F. S.; Mortensen, K.; Almdal, K. *Macromolecules* **1995**, *28*, 3008−3011.
(40) Hamley, I. W.; Pople, J. A.; Fairclough, J. P. A.; Ryan, A. J.; Booth, C.; Yang, Y. W. *Macromolecules* **1998**, *31*, 3906−3911.
(41) Hamley, I. W.; Mortensen, K.; Yu, G. E.; Booth, C. *Macromolecules* **1998**, *31*, 6958−6963.
(42) Almdal, K.; Koppi, K. A.; Bates, F. S. *Macromolecules* **1993**, *26*, 4058−4060.
(43) Phoon, C. L.; Higgins, J. S.; Allegra, G.; van Leeuwen, P.; Staples, E. *Proc. R. Soc. London A: Math. Phys. Eng. Sci.* **1993**, *442*, 221−230.
(44) McConnell, G. A.; Lin, M. Y.; Gast, A. *Macromolecules* **1995**, *28*, 6754−6764.
(45) Hamley, I. W.; Pople, J. A.; Fairclough, J. P. A.; Terrill, N. J.; Ryan, A. J.; Booth, C.; Yu, G. E.; Diat, O.; Almdal, K.; Vigild, M.; Mortensen, K. *J. Chem. Phys.* **1998**, *108*, 6929−6936.
(46) Ackerson, B. J.; Pusey, P. N. *Phys. Rev. Lett.* **1988**, *61*, 1033−1036.
(47) Pusey, P. N.; van Megen, W.; Bartlett, P.; Ackerson, B. J.; Rarity, J. G.; Underwood, S. M. *Phys. Rev. Lett.* **1989**, *63*, 2753−2756.
(48) Sebastian, J. M.; Lai, C.; Graessley, W. W.; Register, R. A.; Marchand, G. R. *Macromolecules 35*, 2700−2706.
(49) Sebastian, J. M.; Lai, C.; Graessley, W. W.; Register, R. A. *Macromolecules 35*, 2707−2713.
(50) Theunissen, E.; Reynaers, H.; Mortensen, K., to be published.
(51) Kraton Polymers Web page: http://www.kraton.com.
(52) Mortensen, K.; Kleppinger, R.; Theunissen, E.; Reynaers, H., manuscript to be submitted.
(53) Hashimoto, T. *Macromolecules* **1994**, *27*, 9002. Suehiro, S.; Saijo, K.; Seto, T.; Sakamoto, N.; Hashimoto, T.; Ito, K.; Amemiya, Y. *J. Synchrotron Rad.* **1996**, *3*, 225−230.
(54) Chen, L. B.; Zukoski, C. F.; Ackerson, B. J.; Hanley, H. J. M.; Straty, G. C.; Barker, J.; Glinka, C. *J. Phys. Rev. Lett.* **1992**, *69*, 688−691.

MA0121013